Electronic Supplementary Material (ESI) for Nanoscale.
This journal is © The Royal Society of Chemistry 2014

On the Mechanical and Electronic Properties of Thiolated Gold Nanocrystals

*K. Smaali[1λ], S. Desbief[1λ], G. Foti[2,3], T. Frederiksen[3,4], D. Sanchez-Portal[2,3], A. Arnau[2,3,5], J.P. Nys[1], P. Leclère[6], D. Vuillaume[1] and N. Clément[1]**

Supplementary Information

[1]Institute of Electronics, Microelectronics and Nanotechnology, CNRS, Avenue Poincaré, 59652, Villeneuve d'Ascq France

[2]Centro de Fisica de Materiales, Centro Mixto CSIC-UPV, Paseo Manuel de Lardizabal 5, Donostia-San Sebastian, Spain

[3]Donostia International Physics Center (DIPC), Paseo Manuel de Lardizabal 4, Donostia-San Sebastián, Spain

[4]IKERBASQUE, Basque Foundation for Science, E-48011, Bilbao, Spain

[5]Depto. de Física de Materiales UPV/EHU, Facultad de Química, Apdo. 1072, Donostia-San Sebastián, Spain

[6]Laboratory for Chemistry for Novel Materials, Center of Innovation and Research in Materials and Polymers (CIRMAP), University of Mons, UMONS, Place du Parc 20, 7000 Mons, Belgium

λ: These authors contributed equally to the study

1 Deformation of the substrate and facets

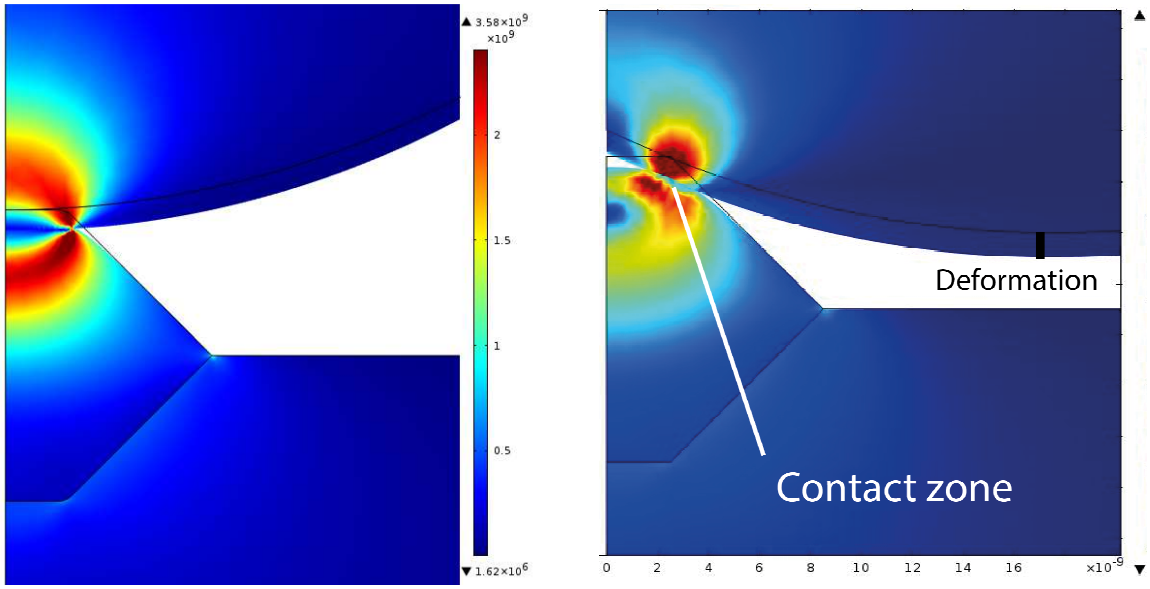

Figure S1 Finite Element Analysis (FEA) illustrating the simulation of a deformation measurement with peakforce AFM when the tip is located above the nanodot (left) and above facets (right). Black lines represent the initial geometry of the system at zero force. We observe a negligible deformation of the substrate in both cases. On the right image, although the contact zone is located only on the edge, the measured deformation (larger than expected) is done at tip center.

2 Tip indentation: “nano” SAM vs large area SAM

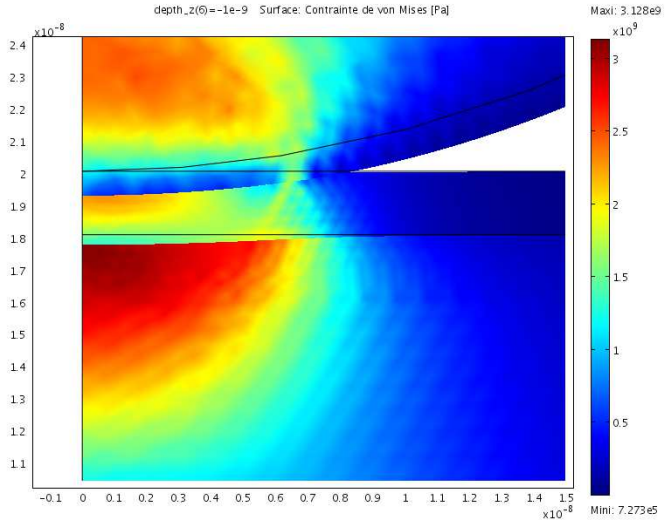

Figure S2a Like previous figure but showing an example of the simulation of the tip indentation in a conventional “large area” SAM. As the tip indents the SAM, the contact area increases.

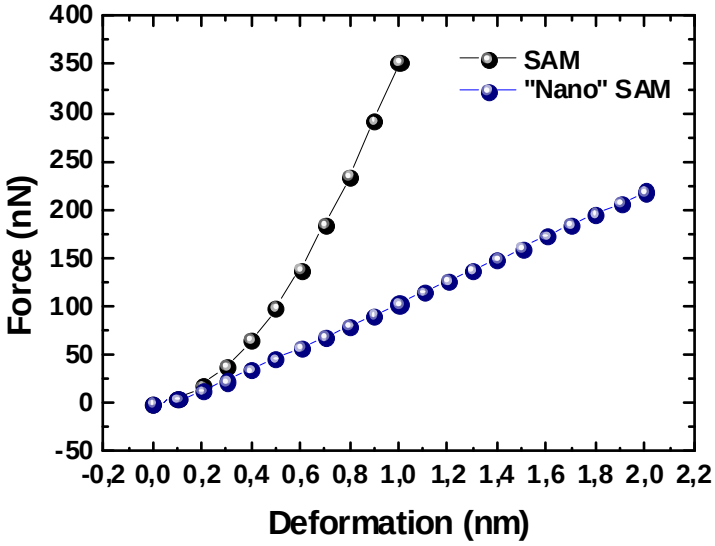

Figure S2b Force-deformation curve obtained by FEA (assuming a Young’s modulus of the SAM of 5 GPa) for a “nano” SAM on a gold nanocrystal and a SAM. Whereas in the first case a linear effect is observed, a parabolic behavior is observed in the second case.

3 Adhesion mapping

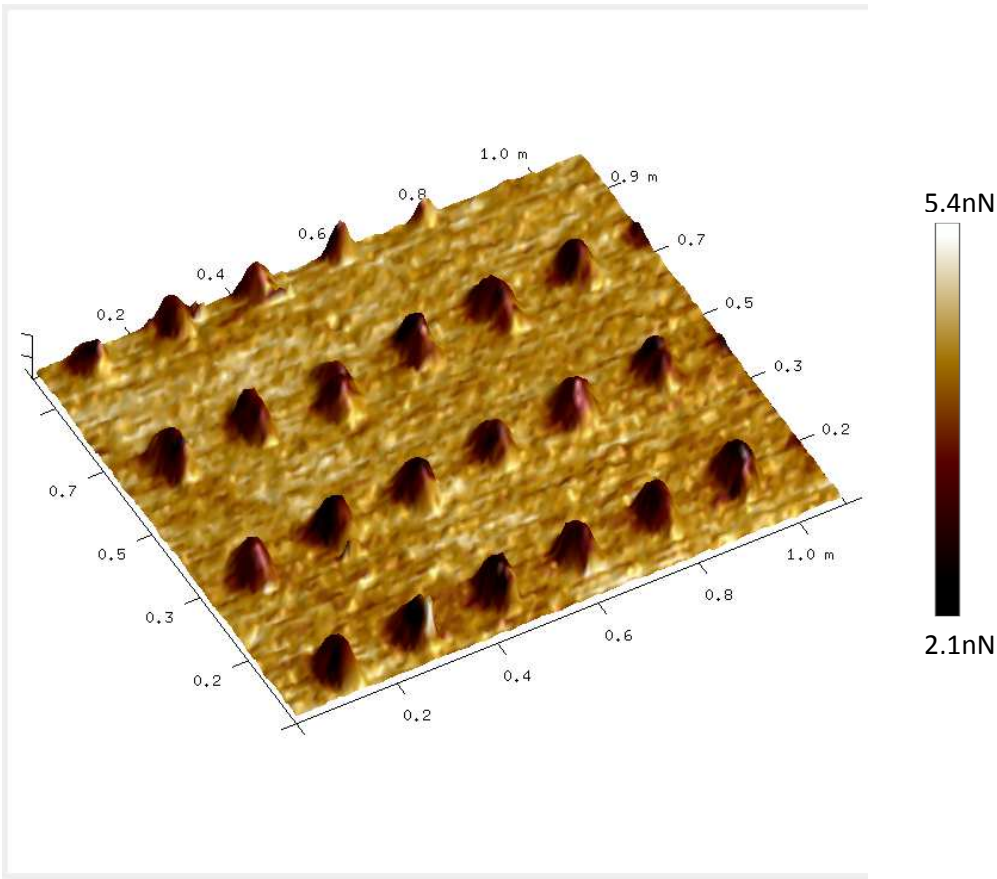

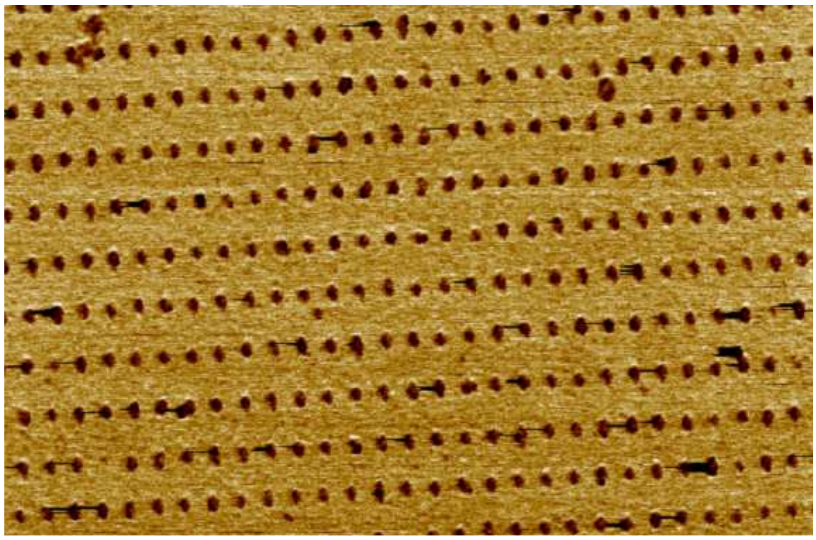

Figure S3 Adhesion-topography coupled images (two different dimensions) of Au nanoparticle (NP) coated with C_8. The adhesion is strongly suppressed on top of the Au NP.

4 SAMs thicknesses

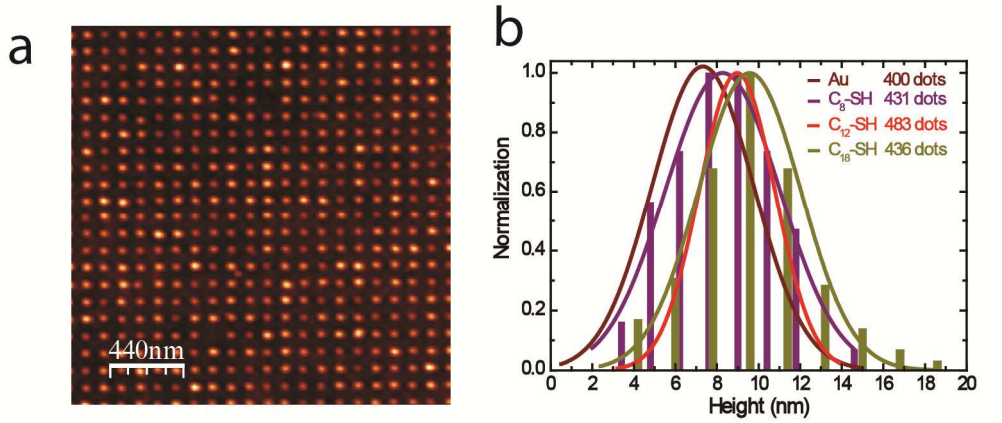

Figure S4 (a) AFM image in tapping mode of an array of gold nanodots covered with C12 molecules (1 μmx 1 μm image with 1024 x 1024 pixels). (b) Normalized height histograms on nanodots and nanodots covered with C_8, C_{12} and C_{18} molecules.

5 Ab-initio density functional method

In order to determine the minimum energy orientation of C_8 and C_{12} we calculated the total energy as a function of the twist and rotational angles respectively [Fig. S5 (a) and (b)] using the relaxed geometry of the isolated molecules assuming a tilt angle θ=30º. Without a proper description of van der Waals (vdW) interactions it is difficult to obtain an accurate estimation of the tilt angle. Therefore, for this initial set of calculations we took this value from the literature, where it is frequently reported [1-3].

We found that the energy landscape shows a periodicity of 60° for Φ (due to the C_6 symmetry axis of the hexagonal lattice) and 180° (C_2 axis of the alkane chain) for Ψ [Fig. S5 (c)].

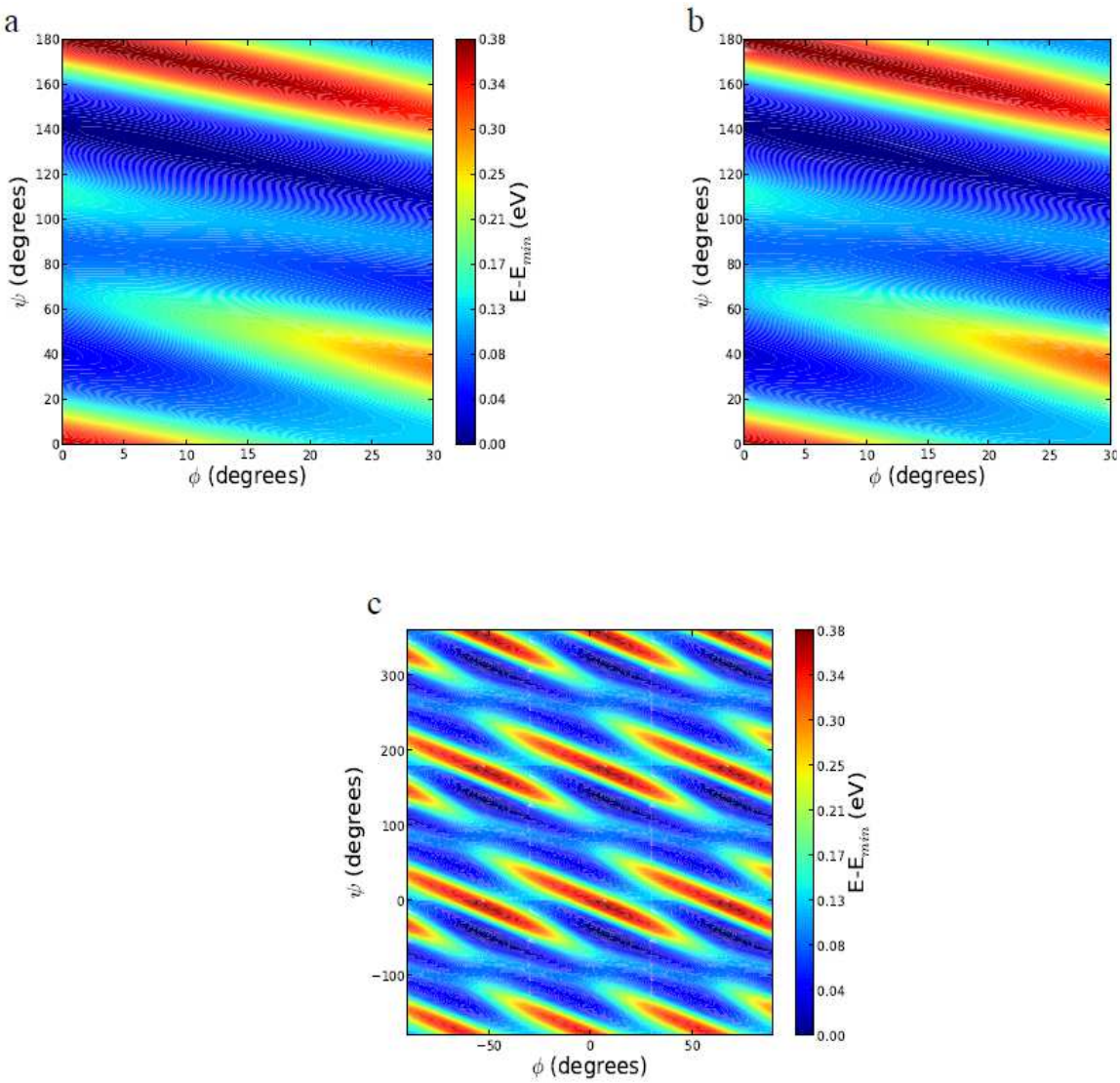

Figure S5 Total energy as a function of twist and rotational angles for a) C_8 and b) C_{12} with PBE functional. The tilt angle θ has been fixed to 30°. In the case of C_8, the minimum of energy is at Φ=9°, Ψ=132° while in the case of C_{12} the minimum of energy is at Φ=8°, Ψ=132°. In panel c) total energy is represented as a periodic repetition of the unit cell defined in the interval: -30≤Φ≤30 and 0≤Ψ≤180.

When using Pedew-Burke-Ernzerhof (PBE)[4] functional we found that, in the case of C_8 the minimum of energy is at Φ = 9°, Ψ = 132° while in the case of C_{12} the minimum of energy is at Φ = 8°, Ψ= 132°. Using a functional that includes vdW corrections[5] the two minima shift in both cases to Φ = 6° and Ψ= 138°. So we found that, if no effects of substrate and anchoring groups are considered and assuming the same coverage (same d=5.05 Å, distance between molecules), C_8 and C_{12} relax to the same minimum energy configuration as already found in a previous work.[6] Note that Φ =30°, Ψ=90°, the configuration that gives a Young modulus E_{sam} within the experimental

range of values, is not far from a minimum of energy. After determining the relevant range for Φ and Ψ, we relaxed four different configurations corresponding to different combinations of Φ and Ψ. We did that using the z-matrix coordinates until residual forces were lower than 0.03 eV/Å and 0.003565 Ry/rad. Then, for each conformation, we tilted the molecule as a rigid rod with respect to the carbon atom of the lower CH_3 group in order to calculate the tilt-vs-force curve. The approximation of tilting the molecule rigidly is justified by two facts: i) the molecule is embedded in a monolayer with small room for bending, and ii) much larger stiffness of the molecules respect to stretching than respect to bending or rotation. We chose this approach of fixing (Φ,Ψ) in order to obtain smooth energy versus tilt angle curves that we can numerically differentiate to get the stress versus tilt. The result shown in Fig. 5 c and d in the paper indicate a similar elastic response of the monolayers formed by C8 and C_{12} molecules.

The independence of the Young modulus on the length of the chain is, for an isolated chain constrained to keep a straight conformation, an expected result (at least for a sufficiently long chain). However, it is more interesting the fact that this length independence still holds for the close-packed layer of chains forming an angle with respect to the direction of the load, and this angle being a function of the applied stress.

Further insight could be provided by looking at the energy surface as a function of Φ and Ψ. For short and long chains we get basically the same potential energy landscape [Fig. S5 a) and b)]. Its derivative with respect to the tilt (which is the force) is the same. This means that, for fixed Φ and Ψ, we expect the same potential energy curve as a function of θ for both C_8 and C_{12} . Using the previous data we can get an estimation of Young's modulus E_{SAM} as function of tilt. The Young's modulus is defined as (notice that this definition extends to finite deformations):

$$E(\theta) = d\sigma/d\varepsilon \qquad \text{(Eq.S1)}$$
$$= 1/A.dF/d\varepsilon$$
$$= 1/A.\cos(\theta_0)/\sin(\theta).dF/d\theta$$

where σ is the stress expressed as a force F per unit area A while ε is the adimensional strain $\varepsilon=(z_0-z)/z_0$ with respect to the equilibrium position $z_0=L_0\cos(\theta_0)$ and L_0 is the length of the molecule.

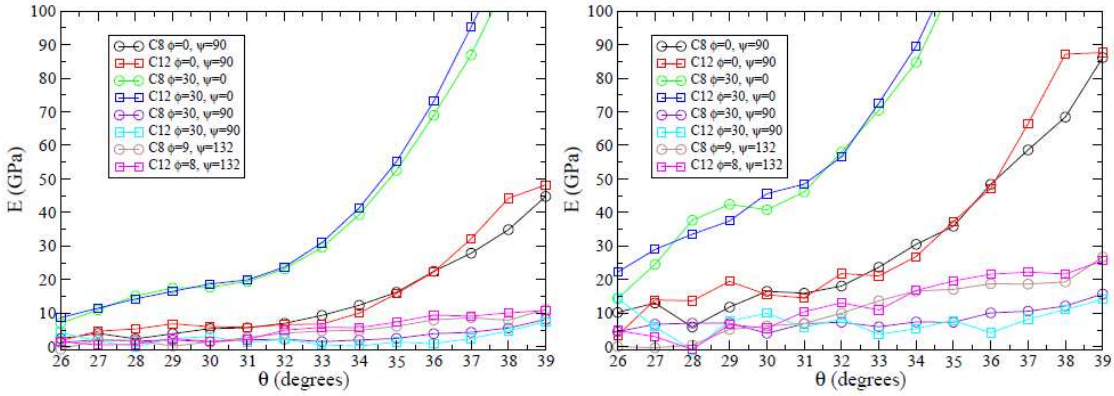

Figure S6 Calculated Young's modulus E(θ) for C_8 and C_{12} as a function of tilt angle using PBE (left)and vdW (right) functional comparison

As we can see from Fig. 3c in the paper Young's modulus depends not only on the tilt angle θ but also on the other two angles Ψ and Φ . When tilting the molecules, due to intermolecular interactions, E_{SAM} increases with a slope which depends on the particular orientation of the molecule. There are no remarkable differences between PBE and vdW calculation. Young's modulus for the minimum energy configurations close to the equilibrium position (θ between 33° and 35°) is between 4.66 GPa and 19.4 GPa. We should stress that these values should be considered as an upper limit of the theoretical prediction. Firstly, since molecules are not fully relaxed for each angle θ, a steeper slope of the force with respect to the tilt is obtained. This means that our results have to be considered as an upper limit of the real values. Secondly, in our calculations we did not consider the effects of both surface and anchoring groups. In Fig. S6 we show the Young's modulus as a function of the angle when using PBE and vdW functional respectively for different (Φ,Ψ) configurations.

6 Normal distribution

If X is a random variable with a normal distribution, then Y=exp(X) has a log-normal distribution; likewise, if Yis log-normally distributed, then log(Y) is normally distributed.

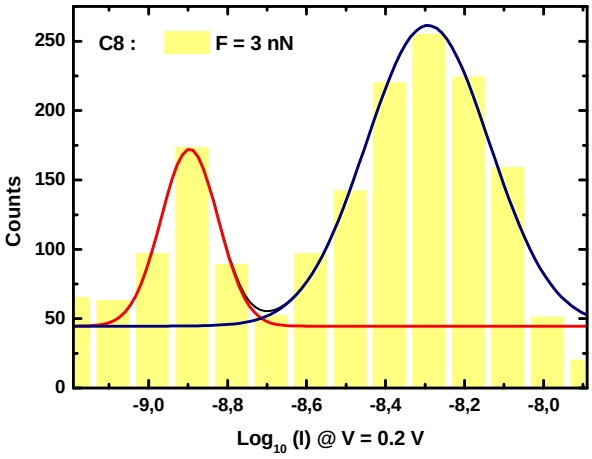

		F (nN) & V = + 0.2 V					
		3		7.5		30	
		Log_{10} (I (A))	FWHM	Log_{10} (I (A))	FWHM	Log_{10} (I (A))	FWHM
C8	HC	-8.29	0.31	-7.90	0.16	-7.71	0.03
	LC	-8.89	0.14	-8.13	0.12	-7.79	0.17
C12	HC	-9.89	0.24	-8.99	0.19	-8.82	0.10
	LC	-10.37	0.34	-9.41	0.36	-8.55	0.17
C18	HC	-	-	-10.44	0.23	-8.84	0.07
	LC	-	-	-10.99	0.26	-8.94	0.02

Figure S7: Top: Log(I) histograms for C_8-coated NPs. The 2 peaks are fitted with log-normal functions. Bottom: Fits results for C_8, C_{12}, C_{18} molecules and different forces are reported in the table.

7 Thermal effects

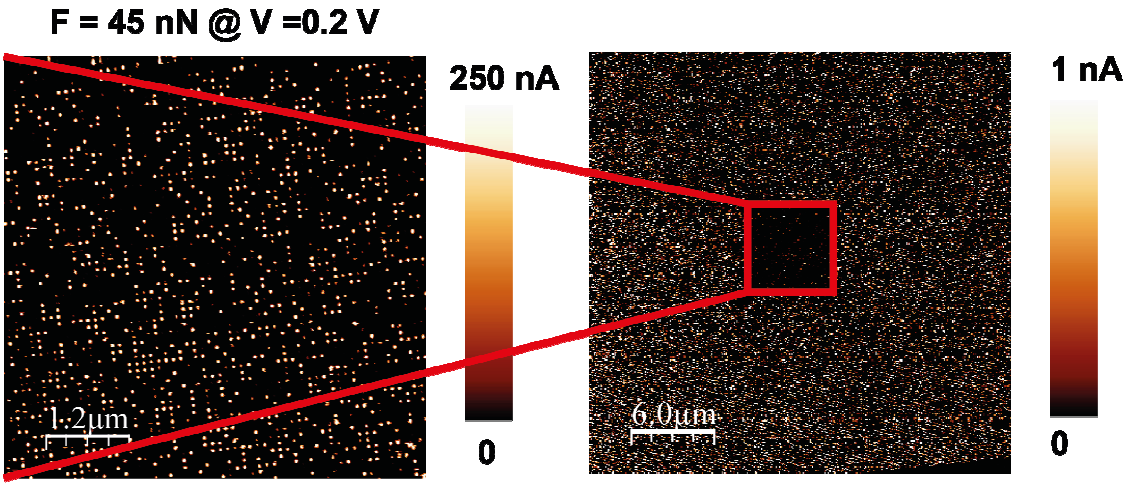

Figure S8 Conducting Atomic Force Microscope (CAFM) image left when a force (~45 nN) and 0.2 V is applied on C_8-coated Au NP. As a result of coupled large force/large current density, sublimation of Au NPs is noticed in a second (enlarged) CAFM image.

8 Transition Voltage Spectroscopy

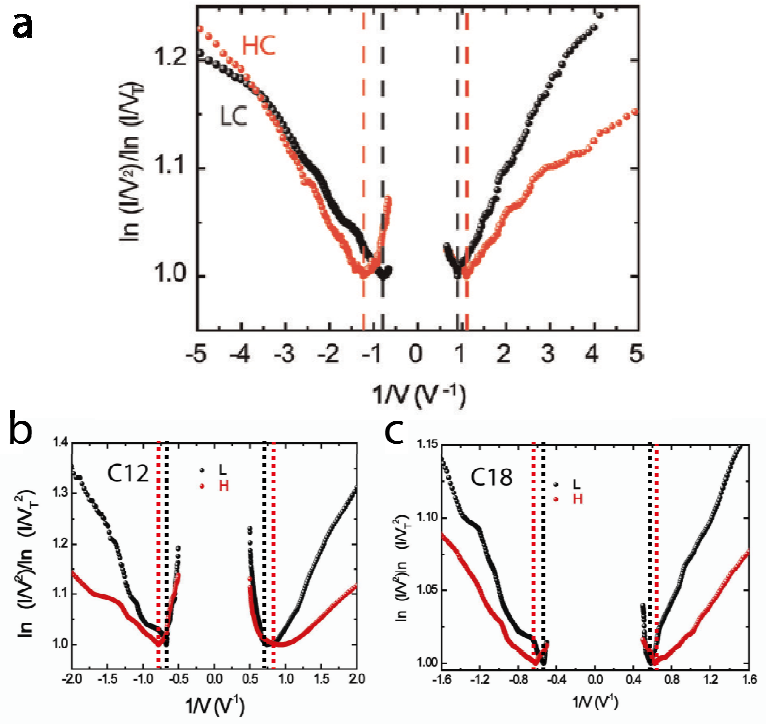

Figure S9 Fowler-Nordheim plots for a) C_8-, b) C_{12}-, c) C_{18}- Au nanocrystals. V_T (minimas in these plots) are symmetric in positive and negative voltages.

9 Kelvin Force Microscopy (KFM)

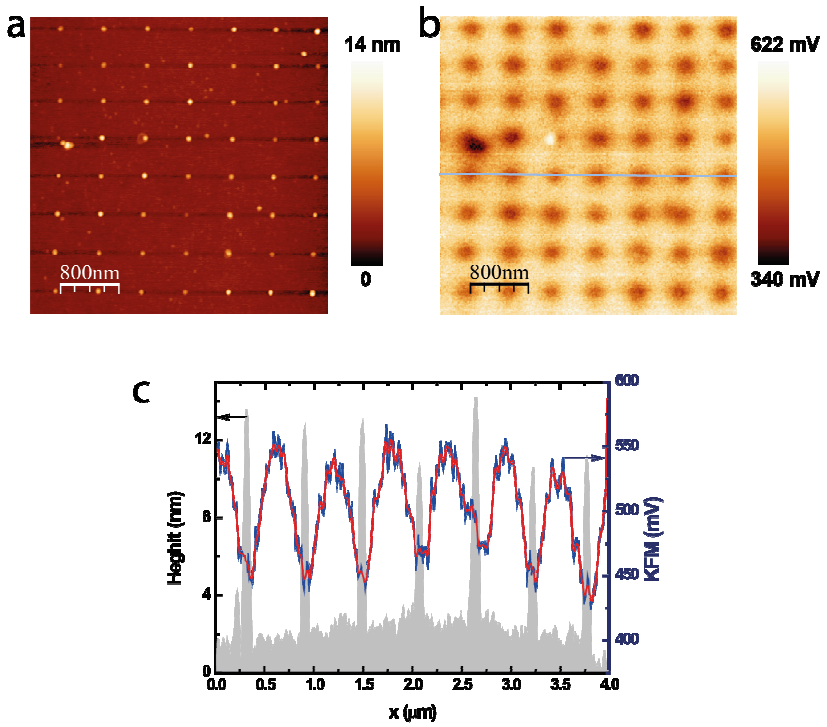

Figure S10 Topographic (a), Kelvin Force Microscope (KFM) (b) and cross section views of both topographic and KFM images (c) for C_8-coated Au NPs.

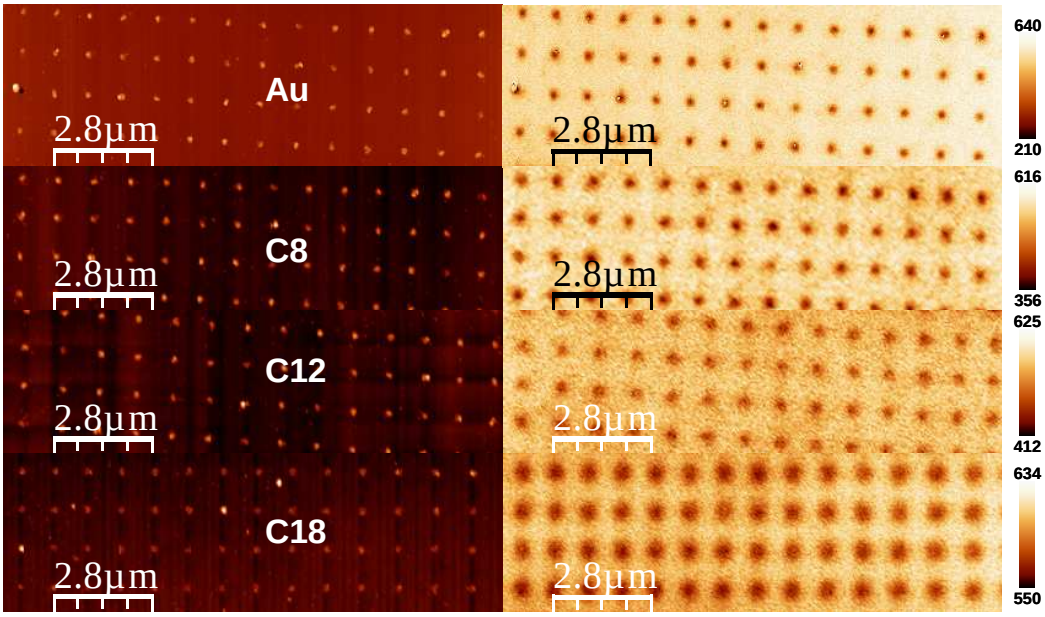

Figure S11 Topographic (left) and KFM (right) images for naked, C_8 -, C_{12}-, C_{18}-Au NPs.

10 Origin C program used for the treatment of C-AFM images on the array of nanodots

The 1st function applies a threshold to put 0 in the matrix below the threshold (removal the background noise). Then, the maximum per dot is obtained by checking the nearest neighbors (function maxi).

```
void Threshold(string strName, double thmin, double thmax, int ibegin, int iend, int jbegin, int jend)
{
	Matrix mm(strName);
	for (int i=ibegin; i<iend; i++)
		for (int j=jbegin; j<jend; j++)
			if ((mm[i][j]<thmin)||(mm[i][j]>thmax)){mm[i][j]=0};
}

void maxi(string strName, int neighbors, int ibegin, int iend, int jbegin, int jend)
{
	Matrix mm(strName);
	for (int i=ibegin; i<iend; i++)
	{
		for (int j=jbegin; j<jend; j++)
		{
			if(mm[i][j]!=0)
			{
				for (int k=¶ 1*neighbors; k<=neighborss; k++)
				{
					for (int l=¶ 1*neighbors; l<=neighbors; l++)
					{
						if (((i+k)>=0)&&((j+l)>=0)&&((i+k)<iend)&&
						((j+l)<iend))
						if(mm[i+k][j+l]>mm[i][j]) {mm[i][j]=0};
					}
				}
			}
		}
	}
	int a=0;
	Worksheet wks;
	wks.Create("histogram.otw");
	WorksheetPage wksp=wks.GetPage();
	wksp.Rename("histogram");
	string str;
	for (int m=ibegin; m<iend; m++)
	{
		for (int n=jbegin; n<jend; n++)
		{
			if (mm[m][n]!=0)
			{
				str.Format("%f",mm[m][n]);
				wks.SetCell(a, 0, str); // set the value to a cell of worksheet
				a++;
			}
		}
	}
}
```

Program call in Origin Labtalk window :
Threshold(Matrixname,threshold_min_nb,threshold_max_nb,0,8192,0,8192);
maxi(Matrixname,nb_neighbors,0,8192,0,8192);
Typically, we use 5 neighbors.

11 Interface dipole

The perpendicular projection of the interface dipole, μ_z, is given by the Helmholtz

equation:

$$\Delta CPD = \frac{N\mu_z}{\varepsilon_0 \varepsilon_{SAM}}$$

where $\Delta CPD = CPD_{SAM} - CPD_{Au}$, N is the surface density of molecules in the SAM, ε_0 is the vacuum dielectric permittivity, ε_{SAM} is the relative permittivity of the SAM. From KFM on naked Au NPs, we have $CPD_{Au} \sim 220$ mV. We chose an average value of 4×10^{14} cm^{-2} for N, assuming a reasonable molecule packing in the SAMs, and $\varepsilon_{SAM} = 2.5$. From the CPD values shown in Fig. 5f, we get μ_z = 0.58D, 0.37D and 0.34D for the C_{18}, C_{12} and C_8 SAMs, respectively.

12 Resicope image

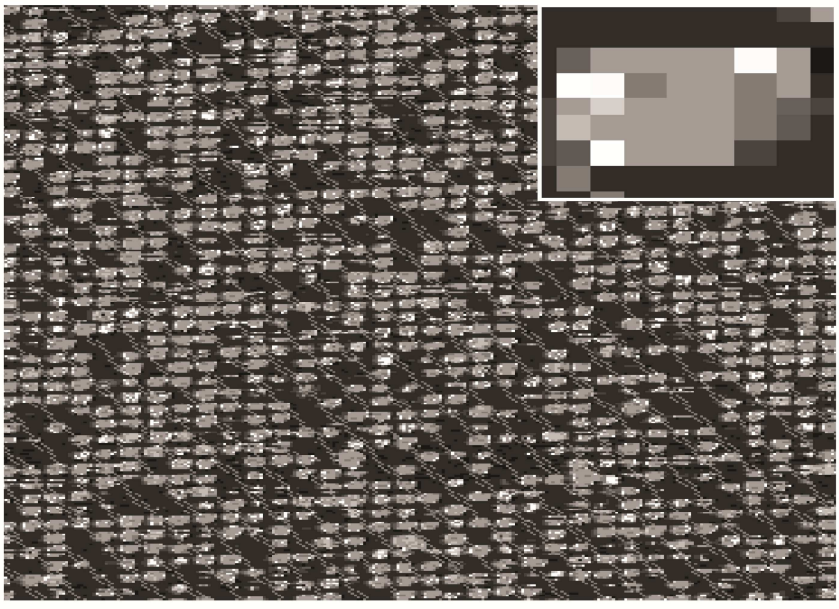

Figure S12. 3.4 µm x 4.3 µm R-AFM image

Resiscope-AFM image (log amplifier) of C_{12} molecular junctions with crystal Au nanodot electrodes. Due to the high scan speed (10 µm/s) parasitic high current levels appear at dot borders (example: white pixels in the dot shown in inset) and the apparent tip curvature radius increased (distance between dots reduced). After thiolation and sample cleaning in the ultrasonic bath, 80-85% of the dots are still there.

[1]L. H. Dubois and R. G. Nuzzo, Annual Review of Physical Chemistry 43, 437 (1992).
[2]C. D. Bain and G. M. Whitesides, Journal of the American Chemical Society 111, 7164 (1989).
[3]M. D. Porter, T. B. Bright, D. L. Allara, and C. E. D. Chidsey, Journal of the American Chemical Society 109, 3559 (1987).
[4]J. P. Perdew, K. Burke, and M. Ernzerhof, Phys. Rev. Lett. 77, 3865 (1996).
[5]M.Dion, H.Rydberg, E.Schr oder, D.C.Langreth, and B.I.Lundqvist. Van der waals density functional for general geometries. Phys. Rev. Lett., 92(24),
2004.
[6]J. G. S. Canchaya, Y. Wang, M. Alcami, F. Martin, and H. F. Busnengo, Phys. Chem. Chem. Phys. 12, 7555 (2010).